Mecánica Computacional Vol. XXIII, pp. 755-772
G.Buscaglia, E.Dari, O.Zamonsky (Eds.)
Bariloche, Argentina, November 2004

NUMERICAL PERFORMANCE OF A MIXED STABILIZED FINITE ELEMENT TECHNOLOGY FOR SOLID MECHANICS. PARALLEL IMPLEMENTATION.

Pablo Sanchez*, Alfredo Huespe†, and Victorio Sonzogni*

*International Center for Computer Methods in Engineering (CIMEC)
INTEC-UNL-CONICET, Güemes 3450, 3000 Santa Fe, Argentina.
e-mail: psanchez@intec.unl.edu.ar, web page: http://www.cimec.org.ar

†Politechnical University of Catalonia (UPC).
Edificio C1, Campus Norte, 08034 Barcelona, Spain.
e-mail: huespe@cimne.upc.es

Key Words: stabilized mixed finite elements, linear-linear interpolation, strain softening, localization problem.

Abstract. *In this work, a mixed stabilized formulation based on the orthogonal sub-grid scale method, is evaluated. The approach considers linear interpolation for displacement and pressure variables. The numerical analysis is particularly addressed to test the formulation behavior under kinematical incompressibility constraints, such as incompressible elasticity problems, limit load determination or strain localization in standard isochoric plasticity models.*

The stabilized scheme is implemented in PETSc-FEM parallel finite element code. A novel preconditioner is used to solve the iterative linear system, comparing its convergence properties with other classical widely used preconditioner.

J2 plasticity model is used as the constitutive law for the proposed examples. The numerical results are compared with standard Galerkin elements and with an alternative stabilized mixed formulation based on pressure stabilized Petrov-Galerkin method.

1 INTRODUCTION

From a computational point of view, the low-order irreducible displacement formulation present several advantages to solve practical problems in solid mechanics. However, it is well known that the numerical response of classical Galerkin elements loses precision (and sometimes also physical sense) for problems involving incompressibility constraints. This situation is typical as much in modelling of near incompressible elasticity as in those constitutive models able to predict isochoric strain plastic rate.

As a result of years of exhaustive investigation, different strategies have been proposed to overcome this problem. In this context, the stabilized finite element methods seems to be a robust and general approaches. Initially they were used in the CFD area (Brooks and Hughes,[1] Johnson et al.,[2] Hughes[3]). The stabilized schemes consist of adding mesh-dependent terms to the usual mixed formulation. Similar concepts, for compressible and incompressible elasticity and plasticity, have been applied to solid mechanics (see for example Hughes and Franca,[4] Franca and Hughes,[5] Lyly and Stenberg,[6] Wall et al.,[7] Klaas et al.[8]).

This study aims at evaluating the numerical performance of a mixed stabilized formulation, recently introduced (Chiumenti et al.,[9,10] Cervera et al.,[11] Valverde[12]), for incompressible elastic problems, perfect Von Mises plasticity and specially for localization phenomenon induced by material instability.

In order to solve large structural problems, the stabilized scheme has been implemented in the "PETSc-FEM" general parallel finite element code (Storti, et al.[13]). Its numerical performance in a 3D test is shown.

This work represents a previous step to obtain a more complex formulation. Our ultimate goal is to develop a finite element technology which also will consider embedded strong discontinuity kinematic to capture collapse mechanisms, typically slip lines, for J2 plasticity with softening. This advanced formulation is subject of another paper.

2 MIXED STABILIZED FORMULATION

Let us consider a solid quasi-static mechanical problem based on linear geometric hypothesis. Next, we introduce some nomenclature to define it: Ω is a open bounded set included in $\mathbb{R}^n$ whose points represent those of a continuum body $\mathbb{B}$ in the reference configuration, Γ is the boundary of Ω which can be split in two subsets $\Gamma_{\boldsymbol{u}}$ and $\Gamma_{\boldsymbol{\sigma}}$ where prescribed displacements $\overline{\boldsymbol{u}}$ and traction $\boldsymbol{t}$ are imposed:

$$\begin{aligned} \boldsymbol{u} &= \overline{\boldsymbol{u}} \quad \text{on} \quad \Gamma_{\boldsymbol{u}} \\ \boldsymbol{\sigma}\cdot\boldsymbol{n} &= \boldsymbol{t} \quad \text{on} \quad \Gamma_{\boldsymbol{\sigma}} \end{aligned} \tag{1}$$

The stress tensor $\boldsymbol{\sigma}$ can be uncoupled into their spherical ($\sigma_m = \frac{1}{3} tr(\boldsymbol{\sigma})$) and deviatoric parts ($\boldsymbol{S} = dev(\boldsymbol{\sigma})$):

$$\boldsymbol{\sigma} = \sigma_m \mathbf{1} + \boldsymbol{S} \tag{2}$$

allowing us to write the equilibrium equations as follows (without inertial forces):

$$\nabla\sigma_m + \nabla\cdot\boldsymbol{S} + \rho\boldsymbol{b} = \boldsymbol{0} \quad \text{on} \quad \Omega \tag{3}$$

being $\mathbf{1}$ the second order identity tensor, $\boldsymbol{b}$ the distributed mass forces and ρ the material density.

Assuming that the mean stress depends uniquely of the strain tensor trace ($\nabla \cdot \boldsymbol{u} = tr(\boldsymbol{\varepsilon})$), the dependence of stresses with the (symmetric gradient of) displacements $\boldsymbol{u}$ can be write as follows:

$$\boldsymbol{\sigma} = \hat{\boldsymbol{\sigma}}(\boldsymbol{u}) = \hat{\sigma}_m(\nabla \cdot \boldsymbol{u})\, \mathbf{1} + \boldsymbol{S}(\boldsymbol{u}) \tag{4}$$

The standard widely used mixed approach to the problem (3), (4) with boundary conditions (1) is based on the set of primary variables $(p, \boldsymbol{u})$, where $p(\boldsymbol{x})$ is the hydrostatic pressure (negative mean stress). According to this formulation, the stress tensor can be computed as:

$$\boldsymbol{\sigma} = -p\, \mathbf{1} + \boldsymbol{S}(\boldsymbol{u}) \tag{5}$$

where both principal variables (p and $\boldsymbol{u}$) should verify the following continuum constraint:

$$p = -\hat{\sigma}_m(\nabla \cdot \boldsymbol{u}) \quad \text{on} \quad \Omega \tag{6}$$

The variational equations of the mechanical problem (3), (5), (6) and (1) can be put in the classical context: find $(p, \boldsymbol{u}) \in L^2(\Omega) \times H^1(\Omega)$, such that:

$$\begin{aligned} \mathcal{L}([p, \boldsymbol{u}]; [q, \boldsymbol{w}]) = &-\langle p; \nabla \cdot \boldsymbol{w} \rangle + \langle \boldsymbol{S}(\boldsymbol{u}); \nabla^s \boldsymbol{w} \rangle - \langle \rho \boldsymbol{b}; \boldsymbol{w} \rangle - \\ &- \int_{\Gamma_{\boldsymbol{\sigma}}} (\boldsymbol{t} \cdot \boldsymbol{w}) d\Gamma_{\boldsymbol{\sigma}} + \langle q; (p + \hat{\sigma}_m(\nabla \cdot \boldsymbol{u})) \rangle = 0 \\ &\forall \boldsymbol{w} \in H^1_0(\Omega) \quad \wedge \quad \forall q \in L^2(\Omega) \end{aligned} \tag{7}$$

where the expression $\langle a; b \rangle = \int_\Omega (a \cdot b) d\Omega$ represents a internal product, $L^2(\Omega)$ includes the square integrable functions in Ω, $H^1(\Omega)$ includes the functions whose first derivative belongs to $L^2(\Omega)$, and $H^1_0(\Omega)$ is a subspace of $H^1(\Omega)$ whose elements vanish on $\Gamma_{\boldsymbol{u}}$.

Let $(p^h, \boldsymbol{u}^h)$, with $p^h \in Q \subset L^2(\Omega^h)$ and $\boldsymbol{u}^h \in \mathcal{V} \subset H^1(\Omega^h)$, be the finite element approaches of the above mentioned fields and $\mathcal{V}$ the finite element approach to $H^1(\Omega^h)$. Using linear interpolation for displacement and pressure, stabilizing terms $\mathcal{S}_{st}$ should be introduced in order to overcome the Babuska-Brezzi condition.[14–16] The discrete form of equation (7) then reads:

$$\begin{aligned} \mathcal{L}([p^h, \boldsymbol{u}^h]; [q^h, \boldsymbol{w}^h]) = &-\langle p^h; \nabla \cdot \boldsymbol{w}^h \rangle + \langle \boldsymbol{S}(\boldsymbol{u}^h); \nabla^s \boldsymbol{w}^h \rangle - \langle \rho \boldsymbol{b}; \boldsymbol{w}^h \rangle - \\ &- \int_{\Gamma_{\boldsymbol{\sigma}}} (\boldsymbol{t} \cdot \boldsymbol{w}^h) d\Gamma_{\boldsymbol{\sigma}} + \langle q^h; (p^h + \hat{\sigma}_m(\nabla \cdot \boldsymbol{u}^h)) \rangle + \\ &+ \mathcal{S}_{st}([p^h, \boldsymbol{u}^h]; [q^h, \boldsymbol{w}^h]) = 0 \qquad \forall \boldsymbol{w}^h \in \mathcal{V}_0 \quad \wedge \quad \forall q^h \in Q \end{aligned} \tag{8}$$

In CFD context, many different stabilization terms $\mathcal{S}_{st}$ have been proposed. The PSPG scheme[17] (pressure stabilizing Petrov-Galerkin, a particular type of GLS procedure) and the PGP method (orthogonal sub-grid pressure gradient projection)[18,19] are shortly described in the following paragraphs. The last scheme has been extended to the elastic solid mechanics context by Chiumenti et al.[9] and used in plasticity by Chiumenti et al.[10,11] and Valverde.[12] These

papers have shown the plausibility of this approach in challenging problems where alternative formulations hardly works well.

Both mentioned procedures consider the term $\mathcal{S}_{st}$ as being directly proportional to a stability coefficient τ which depend on the elastic shear modulus and the finite element size, consequently it can changes from element to other.

2.1 Stabilization term for PSPG scheme

In this case, the stabilization term $\mathcal{S}_{st}$ of equation (8) is defined as:

$$\mathcal{S}_{st}^{PSPG} = -\left\langle \nabla q^h ; \tau^{PSPG} \underbrace{(\nabla \cdot \boldsymbol{\sigma}(p^h, \boldsymbol{u}^h) + \rho \boldsymbol{b}))}_{\boldsymbol{r}^{CE}\text{: residue of the Cauchy equations}} \right\rangle \tag{9}$$

where the factor τ^{PSPG} is chosen as follows:

$$\tau^{PSPG} = \alpha \frac{h^2}{2\mu} \tag{10}$$

being α a positive stability parameter (we have taken $\alpha = \frac{1}{6}$), h the element characteristic size and μ the shear modulus for the elastic regime.

2.2 Stabilization term for PGP scheme

Now, the stabilization term $\mathcal{S}_{st}$ is defined as follows:

$$\mathcal{S}_{st}^{PGP} = \left\langle \nabla q^h ; \tau^{PGP} (\nabla p^h - \boldsymbol{\Pi}^h) \right\rangle \tag{11}$$

where $\boldsymbol{\Pi}^h (\in \mathcal{V})$ is the L^2 projection of discrete pressure gradient (∇p^h) over finite element approximation space ($\mathcal{V}$), as Figure (1) shows:

$$\left\langle (\nabla p^h - \boldsymbol{\Pi}^h) ; \boldsymbol{\eta}^h \right\rangle = 0 \quad ; \quad \forall \boldsymbol{\eta}^h \in \mathcal{V} \tag{12}$$

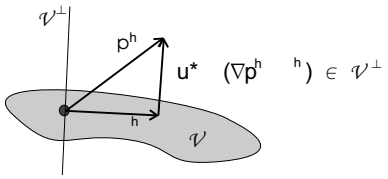

Figure 1: Pressure gradient projection.

Expression (12) should be considered as an additional equation in the variational form (8).

The stabilization parameter τ^{PGP} can be determined element-wise as a function of the element size and the shear modulus:

$$\tau^{PGP} = c \frac{h^2}{2\mu^*} \tag{13}$$

where the scalar coefficient $c = 4$ has been employed by Codina[18] in CFD application. Following Chiumenti et al.,[10] we have adopted the secant shear modulus μ^* in those problems involving J2 type constitutive model.

3 PGP PROCEDURE, ITS NUMERICAL IMPLEMENTATION

Let a finite element method using linear-equal-order interpolation fields for Q and $\mathcal{V}$ be considered. The mechanical problem can be rewritten as: find $p \in Q$ and $\boldsymbol{u} \in \mathcal{V}$, verifying simultaneously (notice that, by legibility, the supra-index h has been removed):

$$-\langle p; \nabla \cdot \boldsymbol{w} \rangle + \langle \boldsymbol{S}(\boldsymbol{u}); \nabla^s \boldsymbol{w} \rangle - \langle \rho \boldsymbol{b}; \boldsymbol{w} \rangle = \int_{\Gamma_{\boldsymbol{\sigma}}} (\boldsymbol{t} \cdot \boldsymbol{w}) d\Gamma_{\boldsymbol{\sigma}} \quad \forall \boldsymbol{w} \in \mathcal{V}_0 \tag{14}$$

$$\langle q; (p + \hat{\sigma}_m(\nabla \cdot \boldsymbol{u})) \rangle + \left\langle \nabla q; \tau^{PGP}(\nabla p - \boldsymbol{\Pi}) \right\rangle = 0 \quad \forall q \in Q \tag{15}$$

$$\langle (\nabla p - \boldsymbol{\Pi}); \boldsymbol{\eta} \rangle = 0 \quad \forall \boldsymbol{\eta} \in \mathcal{V} \tag{16}$$

We also assume a material constitutive model whose mean stress can be described by a linear relation of $tr(\boldsymbol{\varepsilon})$:

$$\hat{\sigma}_m(\nabla \cdot \boldsymbol{u}) = \kappa \nabla \cdot \boldsymbol{u} \tag{17}$$

being κ the bulk modulus.

Using standard matrix notation the interpolated fields, at element level, can be written as:

$$\boldsymbol{u}^e(\boldsymbol{x}, t) = \boldsymbol{N}_{\boldsymbol{u}}^e(\boldsymbol{x}) \hat{\boldsymbol{u}}^e(t) \quad ; \quad \boldsymbol{w}^e(\boldsymbol{x}) = \boldsymbol{N}_{\boldsymbol{u}}^e(\boldsymbol{x}) \hat{\boldsymbol{w}}^e \tag{18}$$

$$p^e(\boldsymbol{x}, t) = \boldsymbol{N}_p^e(\boldsymbol{x}) \hat{\boldsymbol{p}}^e(t) \quad ; \quad q^e(\boldsymbol{x}) = \boldsymbol{N}_p^e(\boldsymbol{x}) \hat{\boldsymbol{q}}^e \tag{19}$$

$$\boldsymbol{\Pi}^e(\boldsymbol{x}, t) = \boldsymbol{N}_{\boldsymbol{u}}^e(\boldsymbol{x}) \hat{\boldsymbol{\Pi}}^e(t) \quad ; \quad \boldsymbol{\eta}^e(\boldsymbol{x}) = \boldsymbol{N}_{\boldsymbol{u}}^e(\boldsymbol{x}) \hat{\boldsymbol{\eta}}^e \tag{20}$$

where $\boldsymbol{N}_u^e$ and $\boldsymbol{N}_p^e$ are the shape function matrices. Furthermore, it is considered that:

$$\nabla^s \boldsymbol{N}_{\boldsymbol{u}}^e = \boldsymbol{B}^e \tag{21}$$

$$\nabla \cdot \boldsymbol{N}_{\boldsymbol{u}}^e = \mathbb{I}^T \boldsymbol{B}^e \tag{22}$$

$$\nabla \boldsymbol{N}_p^e = \boldsymbol{D}^e \tag{23}$$

where $\boldsymbol{B}^e$ is the standard strain-displacement operator and $\mathbb{I}$ the vector representation of the second order identity tensor.

The algorithmic form of equations (14)-(16) can be now expressed as:

$$\begin{cases} \mathop{\mathsf{A}}_{e=1}^{nel} \left[\displaystyle\int_{\Omega^e} \boldsymbol{B}^{eT} \boldsymbol{S}^e(\hat{\boldsymbol{u}}) \, d\Omega^e \right] - \boldsymbol{G}_0 \, \hat{\boldsymbol{p}} = \boldsymbol{f} \\ -\boldsymbol{G}_0^T \, \hat{\boldsymbol{u}} - \left[\dfrac{1}{\kappa} \boldsymbol{M}_p + \boldsymbol{L} \right] \hat{\boldsymbol{p}} + \boldsymbol{H}^T \hat{\boldsymbol{\Pi}} = 0 \\ \boldsymbol{H} \hat{\boldsymbol{p}} - \boldsymbol{M}_{\boldsymbol{u}} \hat{\boldsymbol{\Pi}} = 0 \end{cases} \tag{24}$$

being A the standard finite element assembly operator.

The discrete external force is computed as:

$$\boldsymbol{f} = \mathop{\mathsf{A}}_{e=1}^{nel} \left[\int_{\Omega^e} \rho\, \boldsymbol{N}_{\boldsymbol{u}}^{eT} \boldsymbol{b}^e \; d\Omega^e + \int_{\Gamma_{\boldsymbol{\sigma}}^e} \boldsymbol{N}_{\boldsymbol{u}}^{eT} \boldsymbol{t}^e \; d\Gamma_{\boldsymbol{\sigma}}^e \right] \tag{25}$$

and the matrices $\boldsymbol{G}_0$, $\boldsymbol{M}_p$, $\boldsymbol{M}_{\boldsymbol{u}}$, $\boldsymbol{L}$ and $\boldsymbol{H}$ acquire the following expressions:

$$\boldsymbol{G}_0 = \mathop{\mathsf{A}}_{e=1}^{nel} \left[\int_{\Omega^e} \boldsymbol{B}^{eT} \mathbb{I} \boldsymbol{N}_p^e \; d\Omega^e \right] \tag{26}$$

$$\boldsymbol{M}_p = \mathop{\mathsf{A}}_{e=1}^{nel} \left[\int_{\Omega^e} \boldsymbol{N}_p^{eT} \boldsymbol{N}_p^e \; d\Omega^e \right] \tag{27}$$

$$\boldsymbol{M}_{\boldsymbol{u}} = \mathop{\mathsf{A}}_{e=1}^{nel} \left[\int_{\Omega^e} \boldsymbol{N}_{\boldsymbol{u}}^{eT} \tau^{PGP} \boldsymbol{N}_{\boldsymbol{u}}^e \; d\Omega^e \right] \tag{28}$$

$$\boldsymbol{L} = \mathop{\mathsf{A}}_{e=1}^{nel} \left[\int_{\Omega^e} \boldsymbol{D}^{eT} \tau^{PGP} \boldsymbol{D}^e \; d\Omega^e \right] \tag{29}$$

$$\boldsymbol{H} = \mathop{\mathsf{A}}_{e=1}^{nel} \left[\int_{\Omega^e} \boldsymbol{N}_{\boldsymbol{u}}^{eT} \tau^{PGP} \boldsymbol{D}^e \; d\Omega^e \right] \tag{30}$$

where the 0 subscript accounts the Dirichlet homogeneous boundary condition.

The non-linear equation systems (24) can be solved for every load step using a classical Newton-Raphson procedure. In this circumstances, the extra computational cost due to the introduction of the new field $\boldsymbol{\Pi}$, provides a no competitive scheme if compared with alternative stabilizing method. Following to Codina et al.[18] and Chiumenti et al.[9] a simplified strategy can be introduced to make it more efficient. Considering that the pressure projection gradient does not change significantly in the $(i+1)$ load step, it is possible to solve the alternative system:

$$\begin{cases} \displaystyle\mathop{\mathsf{A}}_{e=1}^{nel} \left[\int_{\Omega^e} \boldsymbol{B}^{eT} \boldsymbol{S}_{(i+1)}^e \; d\Omega^e \right] - \boldsymbol{G}_0\, \hat{\boldsymbol{p}}_{(i+1)} = \boldsymbol{f}_{(i+1)} \\ \displaystyle -\boldsymbol{G}_0^T\, \hat{\boldsymbol{u}}_{(i+1)} - \left[\frac{1}{\kappa} \boldsymbol{M}_p + \boldsymbol{L}_{(i+1)} \right] \hat{\boldsymbol{p}}_{(i+1)} = -\boldsymbol{H}_{(i+1)}^T\, \hat{\boldsymbol{\Pi}}_{(i)} \end{cases} \tag{31}$$

where $\hat{\boldsymbol{\Pi}}_{(i)}$ is evaluated, by considering equation (24-c), once the nonlinear solver has converged for displacement and pressure variables at the (i) load step. At the global level, it is possible to write:

$$\hat{\boldsymbol{\Pi}}_{(i)} = \boldsymbol{M}_{\boldsymbol{u}}^{-1}\, \boldsymbol{H}_{(i)}\, \hat{\boldsymbol{p}}_{(i)} \tag{32}$$

Therefore, the right hand side term of (31-b) can be considered as an external force for this equation. The evaluation of $\hat{\boldsymbol{\Pi}}_{(i)}$, from equation (32), at the end of the step (i), represents the same computational cost as a postprocessing step.

3.1 Parallel implementation topics

This formulation has been implemented in the PETSc-FEM code (Storti et al.[13]). It is a general purpose multi-physics finite element program developed at the CIMEC running on a Beowulf cluster. PETSc-FEM makes use of the PETSc library[20–22] for linear algebra operations, MPI libraries[23] as the communication package and C++ object oriented philosophy.

The PETSc library allows to treat vectors and matrices in a distributed memory environment without dealing explicitly with parallelism. Therefore it performs the allocation of data on the cluster nodes and let the user make calls to subroutines for linear algebra including solving linear equation systems. The global equation system is solved, in this case, by iterative strategies. As a consequence of PGP stabilization procedure, the global system of equation is symmetrical but not definite positive. A GMRES scheme is used for the solution of the global system (GGMRES).

However global iterative methods fail to solve very large systems. It have been found that procedures based on domain decomposition are better suitable for these large problems. These procedures are based on decomposing the whole domain into subdomains in such a way that solving the global system may be split in two phases: i) solving internal subdomain unknowns and ii) solving global interface unknowns. The internal unknowns may be solved concurrently on each computing node by direct methods (based on LU decomposition). The interface unknowns makes part of a global system which is solved by means of iterative methods. Again here a GMRES-based scheme is used. The size of the global interface system is much smaller than that of the global system, and so the condition number is much smaller making suitable the GMRES solver.

Mesh partitioning is performed by using METIS.[24] Decomposing the domain into non-overlapping subdomains leads to the interface problem whose matrix is the Schur complement. This interface problem is solved by iterative methods which will be referred here as IISD (Interface-Iterative/Subdomain-Direct).

In order to improve the efficiency, this interface solver must be preconditioned, and so the condition number of Schur complement matrix is lowered. In this sense, we use an Interface Strip (IS) preconditioner recently developed (Storti et al.[25]). It is based on solving a problem posed in a narrow strip of nodes around the subdomain interfaces so that the high frequencies of Steklov operator can be correctly captured.

The IS preconditioner requires less memory and computational cost than classical Neumann-Neumann preconditioner and its variants. Besides, the width of strip can be used as a parameter to decide how much memory to assign for preconditioning purposes. In the next section we show its convergence capability.

4 NUMERICAL RESULTS

In this section, the numerical performance of the mixed stabilized PGP model is evaluated and compared with the standard Galerkin (STD), the standard unstable mixed formulation (MSTD) and the PSPG stabilization scheme. The first numerical problem, which involves a large number of equations, is solved in parallel mode with iterative strategies. Its numerical performance is here remarked.

4.1 3D Incompressible elasticity test

The first test consist in a near incompressible elastic block (140 x 140 x 100 millimeters) with the following boundary conditions: all displacement are prescribed to zero at the bottom surface, the upper head is glued to a stiff plate which imposes vertical downward displacements ($\delta_y = 7\,[mm]$); free displacements are assumed on the lateral faces. The mechanical parameters are: Young's modulus $E = 2999800\,[MPa]$, Poisson's ratio $\nu = 0.4999$.

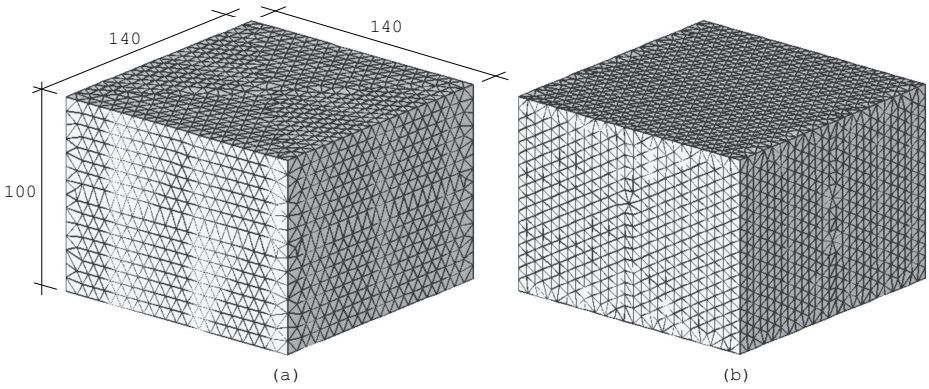

Figure 2: Discretization level: (a) 56000. (b) 90000 tetrahedral elements.

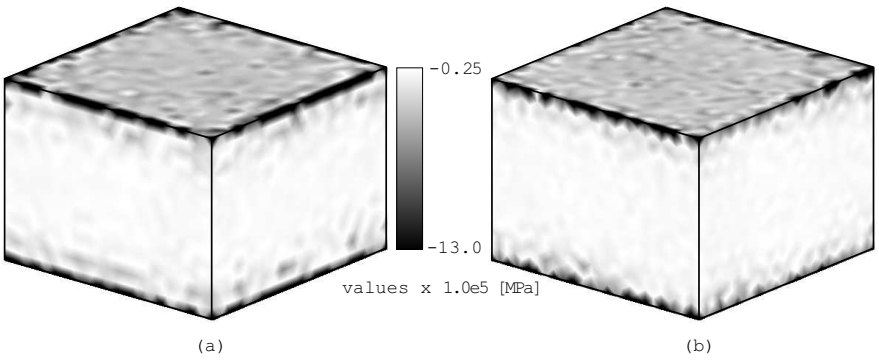

Figure 3: Mean stress maps, MSTD-formulation: (a) 56000. (b) 90000 elements.

Figure (2) shows the discrete models for two unstructured meshes of about 56000 (Figure (2-a)) and 90000 (Figure (2-b)) tetrahedral elements. To test the numerical performance of the par-

allel implementation, this example has been computed solving simultaneously the fully coupled system of equations (24) (entailing approximately 71000 and 112000 equations, respectively).

Figure (3) shows the mean stress field for both meshes and assuming a negligible level of stabilization ($c \approx 0$). This situation represents the response of an unstable mixed standard formulation (MSTD) and severe locking effects are observed. The mean stress oscillation diminishes drastically if the stabilization term $\mathcal{S}_{st}^{PGP}$ is activated, as can be seen from Figure (4), where $c = 1$ has been considered.

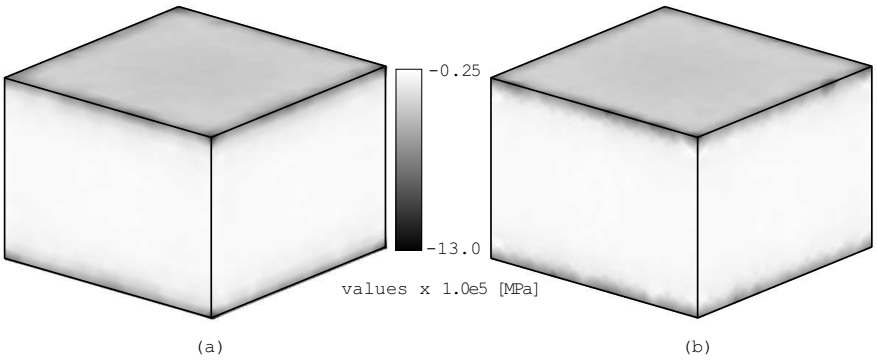

Figure 4: Mean stress maps, PGP-formulation: (a) 56000. (b) 90000 elements.

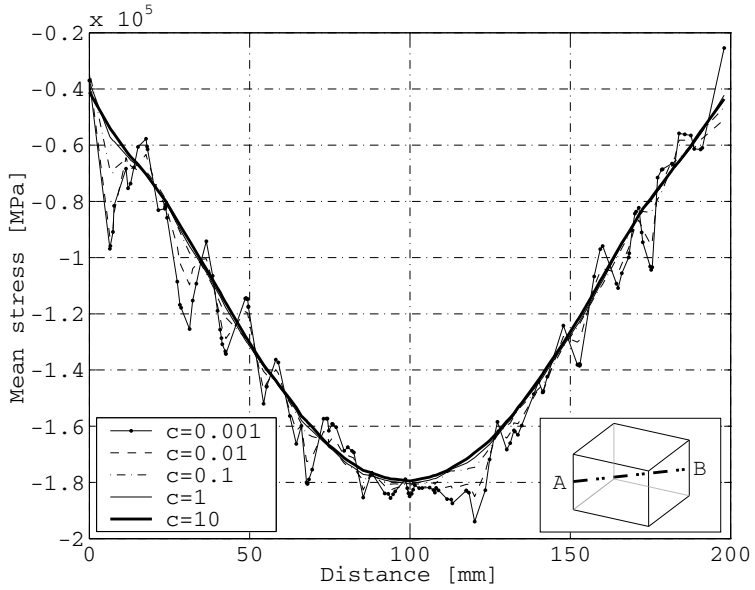

Figure 5: Mean stress curves along of $\overline{AB}$ line, PGP-formulation.

The transition from unstable to stable solution by varying the parameter c can be more clearly evidenced in Figure (5), where the mean stress distributions along the internal line $\overline{AB}$ have been plotted.

Figure (6) shows a comparison between the mean stress curves along the $\overline{AB}$ internal line for the PSPG and PGP stabilization schemes. It can be observed that both solutions are practically identical. According to expressions (10) and (13), the stabilization factors that have been used in this simulation, are:

$$\tau^{PSPG} = \frac{h^2}{12\mu} \quad ; \quad \tau^{PGP} = \frac{2h^2}{\mu} \tag{33}$$

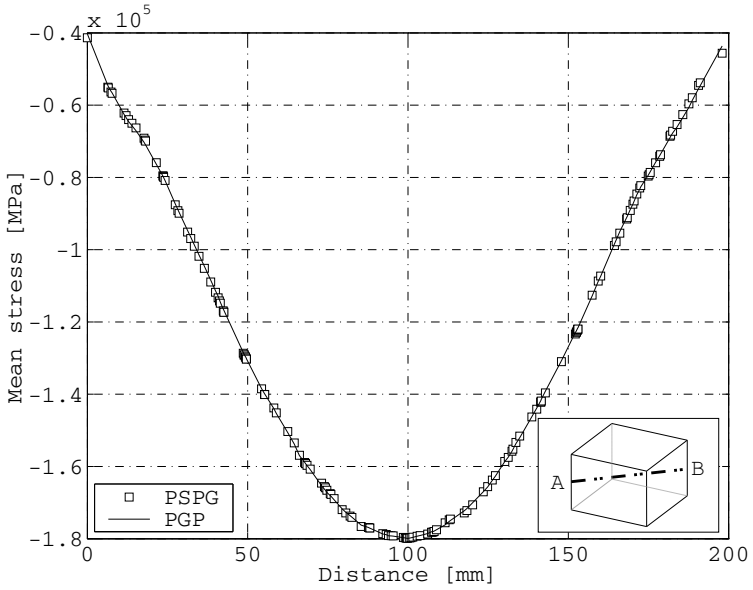

Figure 6: Stabilization procedure comparison: PSPG vs PGP.

Next, we examine the numerical performance of the parallel implementation procedures. Nine nodes of a PC cluster (P4, 2.4 [GHz], 1GB-RAM DDR 333 [MHz]) were utilized. The computational cost comparative analysis for solving the full equation systems (without segregating the $\boldsymbol{\Pi}$ d.o.f.), considers two strategies: *i)* a global iterative GMRES scheme (GGMRES), where the iterative process is carried out on the full system; *ii)* a Schur complement-based procedure, which solves iteratively the interface problem while the internal d.o.f. are solved by direct procedures (IISD). Furthermore, either the standard Jacobi or the Interface Strip (IS) preconditioner are used in the simulations. In the present example the IS preconditioner with a single element layer has been used, and the whole domain is decomposed on nine subdomains, each allocated on a cluster processing node.

Table 1: Time performance, test with 56000 elements.

Solver strategy	**Preconditioner**	**Absolute time**	**Relative time**
GGMRES	Jacobi	64.85 [sec]	3.33
IISD	Jacobi	19.47 [sec]	1.00
IISD	IS	16.93 [sec]	0.87

Table 2: Time performance, test with 90000 elements.

Solver strategy	Preconditioner	Absolute time	Relative time
GGMRES	Jacobi	197.02 [sec]	3.83
IISD	Jacobi	51.49 [sec]	1.00
IISD	IS	45.99 [sec]	0.89

Figure (7) depicts, for the 90000 element test, the required number of iterations to reduce ten orders of magnitude the relative residual norm. The differences between IISD and GGMRES strategy are evident. Using IS preconditioner less iterations are needed and consequently less memory is required to store the Krylov space. The performance measured in total CPU time shows an improvement of approximately 12% with respect to the Jacobi preconditioner (see Table (1) and (2)).

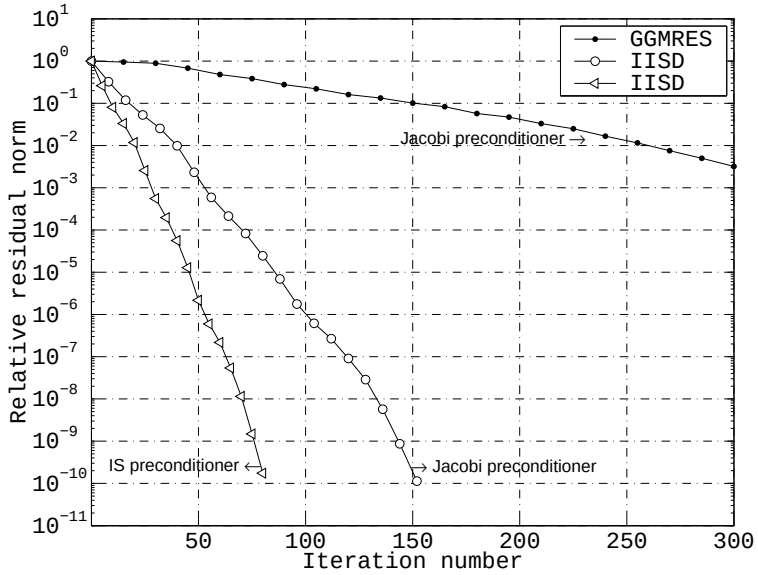

Figure 7: Linear solver convergence, test with 90000 elements.

4.2 Perfect plasticity plane strain test

The plane strain Prandtl's punch test (see Figure (8)) consists of a semi-infinite halfspace vertically loaded by a stiff plate. The collapse mechanism and the corresponding structural limit load, considering a J2 elastic-perfectly plastic material, has been determined analytically (Kachanov,[26] pp. 219). The limit load solution is $\frac{\sigma_N}{\sigma_y} = \frac{2+\pi}{\sqrt{3}}$, where σ_N is the net stress under the punch and σ_y the material yield stress.

Figure (8) depicts the idealized numerical model, geometry relations (dimensions in millimeters) and the boundary conditions. Figure (9) shows two meshes, the unstructured and structured ones. Both of them have approximately 1800 triangular elements. The material properties are: Young's modulus $E = 1.0\,[MPa]$, Poisson's ratio $\nu = 0.499$ (note the quasi-incompressible

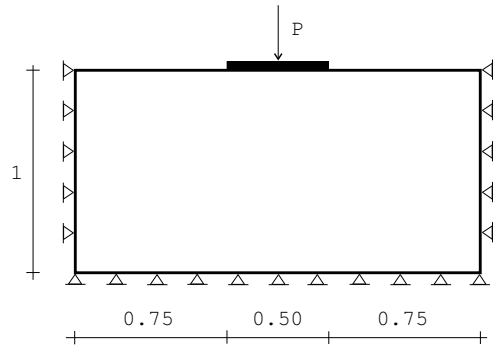

Figure 8: Geometry and boundary condition for 2D plane strain Prandtl test.

elastic response here considered), yield strength $\sigma_y = 0.01\,[MPa]$, perfectly plastic von Mises constitutive model.

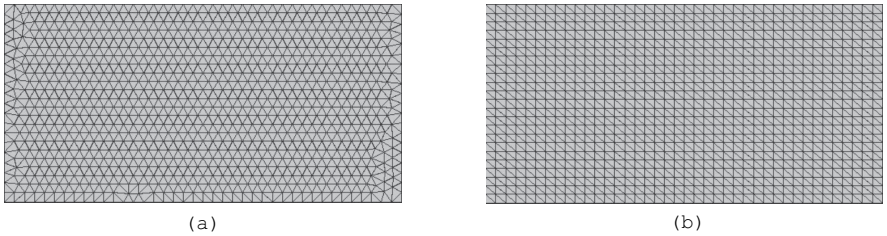

Figure 9: Mesh confi gurations: (a) Unstructured mesh. (b) Structured mesh.

The unstructured configuration has been solved using the linear-linear mixed triangle with the PGP stabilization procedure ($c = 1$) and the standard mixed triangle MSTD ($c \approx 0$). The mean stress values, at the maximum vertical displacement ($\delta_y = 0.10\,[mm]$), are displayed in Figure (10). Again, the standard mixed formulation shows a poor performance characterized by a severe oscillation in the hydrostatic stress field, while the PGP formulation gives a smooth solution.

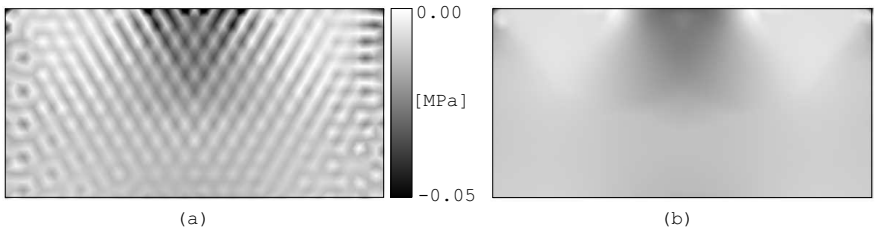

Figure 10: Mean stress maps: (a) MSTD-formulation. (b) PGP-formulation.

The correct capturing of the collapse mechanism for both meshes are analyzed in Figure (11). It shows the equivalent plastic strain fields for the stabilized element (PGP), once the plastic flow is fully achieved. For the unstructured mesh, the failure mechanism observed is

in correspondence with a symmetrical slip line pattern (Figure (11-a)). We remark that the unstructured configuration shows a very approximated symmetrical mesh. Nevertheless, the equivalent plastic strain map, in the structured configuration, does not seem to present a symmetrical response.

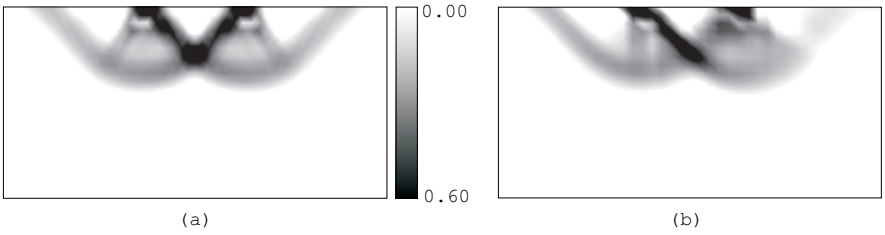

Figure 11: Equivalent plastic strain maps, PGP-formulation: (a) Unstructured mesh. (b) Structured mesh.

Figure (12) compares the total plate reaction vs. the vertical plate displacement curves for both meshes using linear triangles and with different alternatives: the standard Galerkin (STD), the standard mixed (MSTD) and the stabilized mixed (PGP) formulations. As it is expected, the standard Galerkin element shows a response where the limit load is not detected, while the MSTD and PGP formulations, either for unstructured or structured meshes, show a clear limit load. A mesh refining and a larger domain of analysis shall give a more adjusted prediction of the analytical solution.

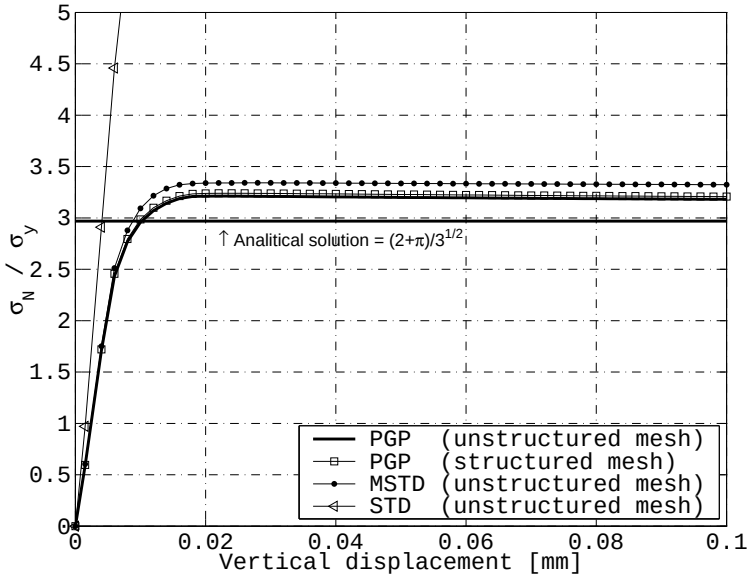

Figure 12: Load-displacement curve.

4.3 2D Strain localization problem test

Finally, a compression test of a prismatic block is considered. This classical plain strain example has been previously used by some authors, to test the ability of finite element formulations for modelling strain localization problems. Von Mises J2 elasto-plastic material model with linear softening is adopted. Under this circumstance, and after the material bifurcation condition has been reached, it should be expected the development of a plastic strain localization band (inclination of about $45°$). We want to analyze the capability of the stabilized PGP triangle to capture this failure mode.

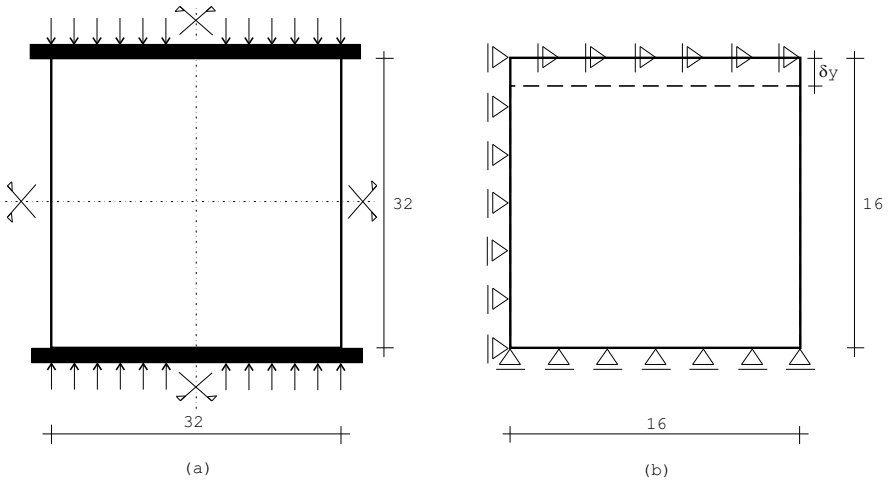

Figure 13: Localization problem: (a) Physical model. (b) Numerical model.

The constitutive model has not been regularized. Therefore the computed load-displacement curve will change with the mesh refining. However, our interest here is to show the mesh-direction independence rather than the mesh-size independence. It should be expected that by using different meshes, with similar element size, the results should be comparable even if the mesh direction changes.

Figure (13-a) shows the geometric proportions of the problem (all dimensions in millimeters). A quarter of the block is considered in the numerical simulation (see Figure (13-b)).

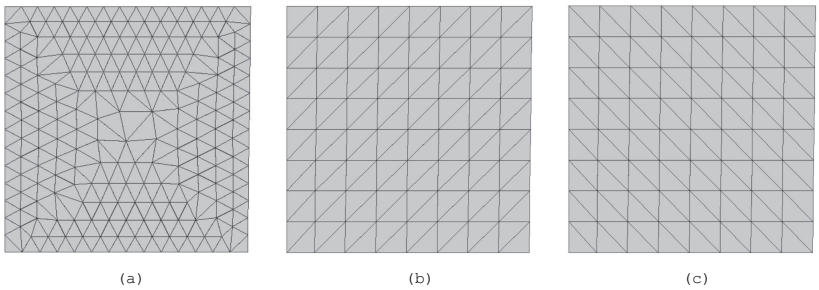

Figure 14: Meshes used in the simulation: (a) 375 elements. (b) 128 elements. (c) 128 elements.

The adopted mechanical parameters are: Young's modulus $E = 3e4\,[MPa]$, Poisson's ratio $\nu = 0.3$, yield stress $\sigma_y = 36\,[MPa]$, softening material modulus $H = -1.8e3$. A small geometric perturbation is also considered in order to determine the strain localization onset point.

Three meshes of linear-linear PGP stabilized triangles ($c = 4$) are considered. The first one, Mesh (a), corresponds to a rather arbitrary distribution of 375 elements. The two remaining meshes are structured arranged of triangles, either following the failure line direction (Mesh (b)), or orthogonal to it (Mesh (c)). Both of them have 128 finite elements (Figure (14)).

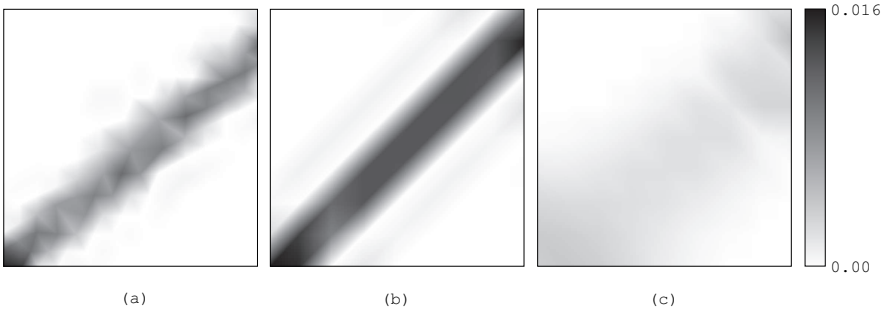

Figure 15: Equivalent plastic strain maps.

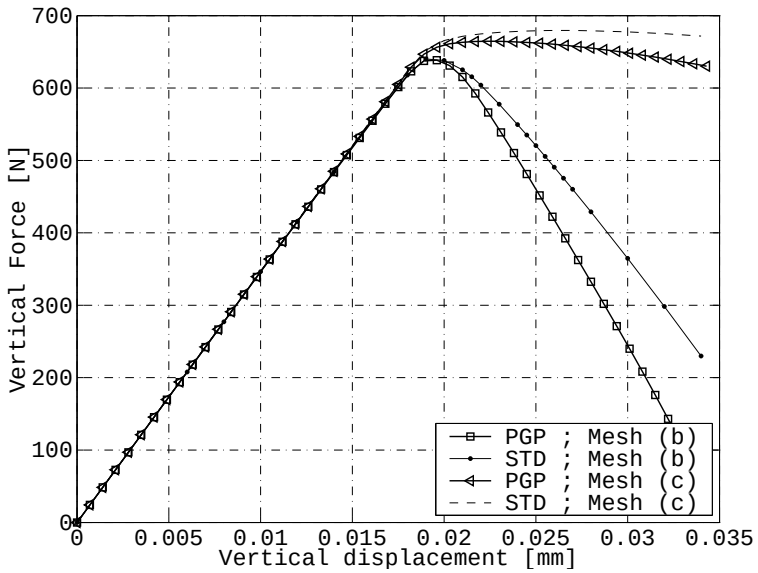

Figure 16: Load-displacement curve.

The performance of the PGP elements in this test can be evaluated by comparing the equivalent plastic strain field (see Figure (15)) and the load displacement curves (Figure (16)) obtained with the meshes (b) and (c). Solution for the mesh (a) is not relevant for the load-displacement

curve comparisons. We can observe that both responses (b) and (c) are clearly different. However, we remark that they represent two extreme conditions. In general, when arbitrary meshes will be used, it should be expected a response like that of Figure (15-a), which display a correct trend for the slip line mode capturing.

5 CONCLUSIONS

We have evaluated a stabilized mixed finite element formulation with equal-low-order (linear) interpolation which shows good performances for solving incompressible solid mechanics problems.

If compared with displacement irreducible formulations, it should be considered the extra computational cost introduced by the additional degree of freedom per node corresponding to the pressure field. However the good performance displaying the linear triangles, and mainly the tetrahedral in 3D cases, makes more than acceptable its use. The treatment of the vectorial field $\boldsymbol{\Pi}$ does not introduce an appreciable computational cost, because it could be treated as an additional smoothing step, once every Newton step has converged.

Its parallel implementation have also shown good performance when the subdomain partitioning method jointly with the Interface-Iterative/Subdomain-Direct technique (IISD) and Interface Strip (IS) preconditioner is used, even though the complete system is solved (i.e. for displacement, pressure and pressure gradient projection d.o.f.).

Using biased meshes, we have observed some mesh-dependence in the plastic localization modelling. The stabilized element conserves the excessive rigidity that shows the standard element, inducing plastic strain dissipation. Probably this deficiency is associated to that neither the mixed formulation nor the stabilization technique, have modified substantially the kinematic of the linear base element, indispensable condition to capture the failure mechanism.

The future work will be dedicated indeed to enrich the element kinematics, incorporating incompatible deformation modes, following the regularized strong discontinuities approach.

REFERENCES

[1] A. N. Brooks and T. J. R. Hughes. Streamline upwind/Petrov-Galerkin formulations for convection dominated flows with particular emphasis on the incompressible Navier-Stokes equations. *Computer Method in Applied Mechanics and Engineering*, **32**, 199–259 (1982).

[2] C. Johnson, U. Nävert, and J. Pitkäranta. Finite element methods for linear hyperbolic problems. *Computer Method in Applied Mechanics and Engineering*, **45**, 285–312 (1984).

[3] T. J. R. Hughes, L. P. Franca, and M. Balestra. A new finite element formulation for computational fluid dynamics: V. Circumventing the Babuska-Brezzi condition: A stable Petrov-Galerkin formulation of Stokes problem accommodating equal-order interpolation. *Computer Method in Applied Mechanics and Engineering*, **59**, 85–99 (1985).

[4] T. J. R. Hughes and L. P. Franca. A mixed finite element formulation for Reissner-Mindlin plate theory: uniform convergence of all higher-order spaces. *Computer Method in Applied Mechanics and Engineering*, **67**, 223–240 (1988).

[5] L. P. Franca and T. J. R. Hughes. Two classes of mixed finite element methods. *Computer Method in Applied Mechanics and Engineering*, **69**, 89–129 (1988).

[6] M. Lyly and R. Stenberg. Stabilized mitc plate bending elements. In *Proc. of 2nd Int. Conf. on Computational Structures Technology*, pages 11–16, Athens, Greece, (1994).

[7] W. A. Wall, M. Bishcoff, and E. Ramm. Stabilization techniques for fluid and structural finite elements. *Computational Mechanics, New Trends and Applications, CIMNE, Barcelona, Spain*, (1998).

[8] O. Klaas, A. Maniatty, and M. S. Shephard. A stabilized mixed finite element method for finite elasticity. Formulation for linear displacement and pressure interpolation. *Computer Method in Applied Mechanics and Engineering*, **180**, 65–79 (1999).

[9] M. Chiumenti, Q. Valverde, C. Agelet de Saracibar, and M. Cervera. A stabilized formulation for incompressible elasticity using linear displacement and pressure interpolations. *Computer Method in Applied Mechanics and Engineering*, **191**, 5253–5264 (2002).

[10] M. Chiumenti, Q. Valverde, C. Agelet de Saracibar, and M. Cervera. Una formulación estabilizada para plasticidad incompresible usando triangulos y tetraedros con interpolaciones lineales en desplazamientos y presiones. *Métodos Numéricos en Ingeniería V*, (2002).

[11] M. Cervera, M. Chiumenti, Q. Valverde, and C. Agelet de Saracibar. Mixed linear/linear simplicial elements for incompressible elasticity and plasticity. *Computer Method in Applied Mechanics and Engineering*, **192**, 5249–5263 (2003).

[12] Q. Valverde. *Elementos estabilizados de bajo orden en mecánica de sólidos*. PhD thesis, UPC, ETSCCP, Barcelona, Spain, (2002).

[13] M. Storti, N. Nigro, and R. Paz. *PETSc-FEM A general purpose, parallel, multy-physics fem program*. International Center of Computational Method in Engineering (CIMEC), http://www.cimec.org.ar/petscfem/.

[14] I. Babuska. Error boudns for finite element methods. *Numerical Mathematics*, **16**, 322–333 (1971).

[15] F. Brezzi. On the existence, uniqueness and aproximation of saddle point problems arising from lagrangian multipliers. *RAIRO*, **8-R2**, 129–151 (1974).

[16] F. Brezzi and M. Fortin. *Mixed and hybrid finite element methods*. Springer, Berlin, Heidelberg, New York, (1991).

[17] T. E. Tezduyar, S. Mittal, S. E. Ray, and R. Shih. Incompressible flow computations with stabilized bilinear and linear equal order interpolation velocity-pressure elements. *Computer Method in Applied Mechanics and Engineering*, **95**, 221–242 (1992).

[18] R. Codina. Stabilization of incompressibility and convection through orthogonal subscales in finite element method. *Computer Method in Applied Mechanics and Engineering*, **190**, 1579–1599 (2000).

[19] R. Codina and J. Blasco. Stabilized finite element method for the transient navier-stokes equations based on a pressure gradient projection. *Computer Method in Applied Mechanics and Engineering*, **182**, 277–300 (2000).

[20] Satish Balay, Kris Buschelman, William D. Gropp, Dinesh Kaushik, Matt Knep-

ley, Lois Curfman McInnes, Barry F. Smith, and Hong Zhang. Petsc home page. http://www.mcs.anl.gov/petsc, (2001).

[21] Satish Balay, Kris Buschelman, William D. Gropp, Dinesh Kaushik, Matt Knepley, Lois Curfman McInnes, Barry F. Smith, and Hong Zhang. Petsc users manual. Technical Report ANL-95/11 - Revision 2.1.5, Argonne National Laboratory, (2002).

[22] Satish Balay, William D. Gropp, Lois Curfman McInnes, and Barry F. Smith. Efficient management of parallelism in object oriented numerical software libraries. In E. Arge, A. M. Bruaset, and H. P. Langtangen, editors, *Modern Software Tools in Scientific Computing*, pages 163–202. Birkhauser Press, (1997).

[23] W. Gropp, E. Lusk, and A. Skeljumm. Using mpi: Portable parallel programming with the message passing interface. Technical report, MIT Press, (1995).

[24] G. Karypis and V. Kumar. Metis 3.0: Unstructured graph partitioning and sparse matrix ordering system, (1997).

[25] M. Storti, L. Dalcin, R. Paz, A. Yommi, V. Sonzogni, and N. Nigro. An interface strip preconditioner for domain decomposition methods. *Journal of Computational Methods in Sciences and Engineering*, (in press) (2003).

[26] L. M. Kachanov. *Foundation of the theory of plasticity*. North-Holland Pub. Co., Neetherlands, (1971).